International Journal of Rock Mechanics & Mining Sciences ▮ (▮▮▮▮) ▮▮▮–▮▮▮

Contents lists available at ScienceDirect

International Journal of Rock Mechanics & Mining Sciences

journal homepage: www.elsevier.com/locate/ijrmms

Numerical modelling of two stoping methods in two Indian mines using degradation of c and mobilization of φ based on Q-parameters

N. Barton [a], S.K. Pandey [b,*]

[a] Nick Barton & Associates, Norway
[b] Rock Mechanics, Hindustan Zinc, Udaipur, India

ARTICLE INFO

Article history:
Received 27 May 2010
Received in revised form
19 May 2011
Accepted 11 July 2011

Keywords:
Q
Q_c
Cohesion component
Frictional component
Displacements
Modulus
Depth dependence

ABSTRACT

Two Indian mines are the subject of a comparative study of a strain-softened Hoek–Brown and FLAC 3D modelling, and a novel 'c then tan φ' strain-softening-strain-mobilization approach, using Q-system based input data. This approach is also used with FLAC 3D, using identical stope geometries. The parameters *CC* and *FC*, denoting the cohesive component and frictional component of shear strength, are extracted directly from the Q-logging and knowledge of *UCS*, and are the source of the peak values. Measured deformations, or the strains recorded over the total length of pre-mining installed MPBX, are compared and effectively calibrate the models, in view of the very similar deformations obtained from empirical formulations based on Q using the competence factor approach, as in SRF. The 'c then tan φ' approach appears to give the most realistic match to observations in the mines, including the modelling of a shear band within the back or roof of a stope, rather than at the surface of the stope. The Q-based approach also uses a depth-dependent modulus, and this is perhaps the reason why the strain-softened Hoek–Brown model, without this stiffening with depth, shows 'global failure' in a second mine having a wider range of depths within one model, and many openings, since modulus is not increased in standard-method approaches.

© 2011 Elsevier Ltd. All rights reserved.

1. Introduction

Determination of input parameters for numerical modelling of rock masses, though apparently made 'simple' if one follows the GSI-based Hoek–Brown formulations and standard commercial software, is inevitably a very poorly quantified area of rock mechanics, when one considers the actual complexity and variation within any given rock mass. Those whose job it is to log core, mining drifts or tunnel walls, and record the variability, know they are committing a gross simplification if they later have to choose, or allow modellers to apply, single *RMR*, Q or *GSI* values, even for single domains.

The geotechnical behaviour of the rock mass, whether of the real variably jointed-partly intact medium, modelled with different joint-set properties in UDEC or 3DEC (including numerically glued 'joints'), but especially when simplified as an isotropic continuum, is inevitably rather poorly quantified. This is despite the 'good feeling' one may have in seeing nicely defined linear or non-linear strength envelopes. Actual deformation and failure modes are a subject of great uncertainty, and controversy, especially in the case of attempted 'continuum' modelling, forced on us 'by the scale of the problem'.

A long time ago, in the late 1960s, there was a move to try to advance beyond the confines of continuum modelling, and focus on the possible actual effects of jointing on the performance and reinforcement needs of rock excavations, be they tunnels, stopes, slopes or dam abutments. Thanks to the late 1960s modelling developments of Goodman and his colleagues with joint elements in FEM codes, immediately followed by Cundall, first with μDEC, then UDEC and later with 3DEC, this focus on greater reality could be fulfilled by an increasing number of rock mechanics practitioners around the world. However, utilizing these codes correctly, with realistic input data, including geometric aspects, needs experience, time and therefore budgets to match. Furthermore 'the scale of the problem', at least in mining, still causes the need to approximate with continuum modelling and elasto-plastic behaviour approximation. This 'fall-back' method, used only because of necessity, is also reported here, but with some important differences in relation to conventional methods of developing input data and its application in the models. Promising trends are indicated.

2. Shear strength of rock masses is a non-trivial subject

The conventional addition of cohesion (c) and the tangent of friction angle (tan φ), in continuum models, either in linear Mohr–Coulomb form, or in a non-linear Hoek–Brown formulation, is unfortunately suspect, when one considers that the

* Corresponding author. Tel.: +919413094531.
E-mail addresses: Suneet.Pandey@vedanta.co.in, s_k_pande@yahoo.co.in (S.K. Pandey).

1365-1609/$ - see front matter © 2011 Elsevier Ltd. All rights reserved.
doi:10.1016/j.ijrmms.2011.07.002

cohesive component, representing some form of quite complex small-strain fracturing of the intact rock, may be a necessary precursor to the mobilization, at larger 'strain', of the non-linear frictional strength of the newly fractured surfaces, and of various joint planes within one or more sets of the pre-existing jointing. The stepped failure surfaces seen in many rock slope failures, following rupture of 'intact bridges' (at small strain), are presumably good near-surface examples of this.

The two (or three) classes of discontinuities involved in post-peak behaviour (natural and induced) will also have quite different sets of shear strength properties. For instance the new failure surfaces, if described with *JRC, JCS* and φ_r, might have, respective, numbers (at small scale) like 18 to 22, 100 to 150 MPa and 30° to 32° (i.e. rough and unweathered and strongly dilatant), compared to perhaps 4 to 8, 50 to 100 MPa and 27° to 29° for potentially weathered joint sets, or perhaps $J_r/J_a=(1 \text{ to } 2)/4$ for any clay-coated discontinuities, that might also be involved in post-peak behaviour. The dilatancy obviously reduces strongly between these three groups of discontinuities. Furthermore, each of the above types of discontinuities are features that begin to resist shearing at considerably larger strains/deformations than is the case for the also strongly dilatant failure of the 'intact bridges'. Why, therefore, are we *adding c* and tan φ in 'continuum' models, making them even poorer representations of the strain-and-process-sensitive reality?

Even ignoring the above reality of the discontinuous and inhomogeneous failure-mode complexity, input data for some continuum codes nevertheless seem to be considerably more complex (e.g., Table 1) than for discontinuum codes, where JRC_0, JCS_0, φ_r, L_0 and L_n and use of just two Barton–Bandis scaling equations, are sufficient to develop the key strength and deformation estimates (L_0 and L_n are lab-scale and in situ scale block sizes). As will be seen in Table 1, the deformation modulus is estimated from *Q* and *UCS* (L_0 and L_n are lab-scale and in situ scale block size).

The correlations proposed in Ref. [1] for estimating the depth-dependent deformation modulus E_m, cohesive component ($CC \approx c$) and the frictional component ($FC \approx \varphi$) based mostly on '*Q*', are listed in the right-hand column of Table 1. In addition, links to the depth dependent seismic P-wave velocity were proposed (see Fig. 1), which have been further documented in wide-ranging reviews in Ref. [2].

Table 2 shows an example of the sort of numbers that can be expected with a variety of rock masses. These key parameter

Table 1
Left: the remarkable complexity of the algebra for estimating c' and φ' and σ'_{cm} with Hoek–Brown based formulations, but with E_m as a more recognisable though complex empirical formulation. Right: the surprising but possibly over-simplified formulations derived by 'splitting' the existing Q_c formula from Barton [1] (where $Q_c=Q\sigma_{ci}/100$, with σ_{ci} expressed in MPa. Note that γ is rock density in gm/cc).

$E_m(GPa)=(1-\frac{D}{2})\sqrt{\frac{\sigma_{ci}}{100}}\times 10^{(GSI-10)/40}$	$E_m \approx 10\times Q_c^{1/3}$
$\sigma'_{cm}=\sigma_{ci}\times\frac{(m_b+4s-a(m_b-8s))\ (m_b/4+s)^{a-1}}{2(1+a)\ (2+a)}$	$\sigma_{cm}\approx 5\gamma\ Q_c^{1/3}$
$\varphi'=a\sin\left[\frac{6am_b(s+m_b\sigma'_{3n})^{a-1}}{2(1+a)(2+a)+6am_b\ (s+m_b\sigma'_{3n})^{a-1}}\right]$	$\varphi\approx\tan^{-1}\left(\frac{J_r}{J_a}\times\frac{J_w}{1}\right)$
$c'=\frac{\sigma_{ci}[(1+2a)s+(1-a)m_b\sigma'_{3n}]\ (s+m_b\sigma'_{3n})^{a-1}}{(1+a)\ (2+a)\sqrt{1+(6am_b(s+m_b\sigma'_{3n})^{a-1})/((1+a)\ (2+a))}}$	$c\approx\left(\frac{RQD}{J_n}\times\frac{1}{SRF}\times\frac{\sigma_c}{100}\right)$
where	*Clear limitations but simple*
$\sigma_{3n}=\sigma'_{3\ max}/\sigma_{ci}$ (+GSI+a+s+m_b relations)	

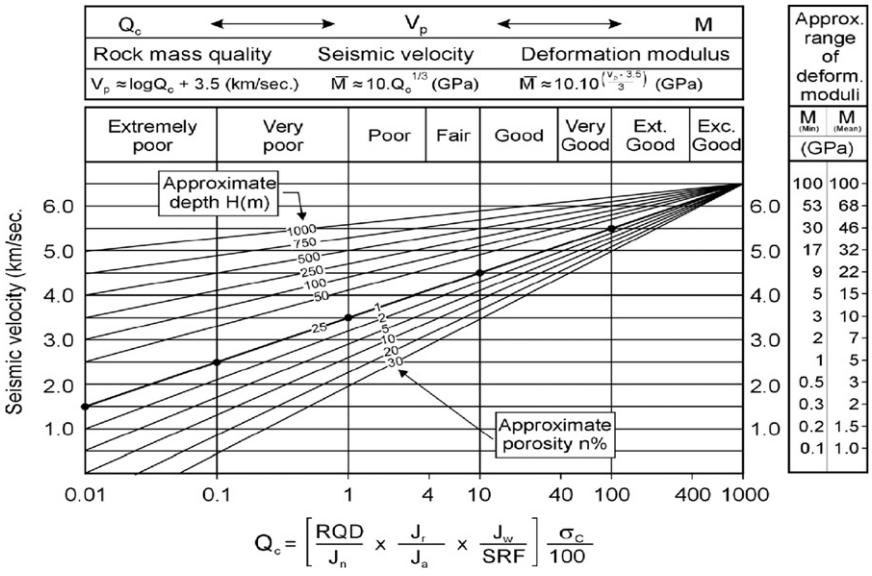

Fig. 1. Inter-correlation of V_P and deformation modulus *M* (or E_m) with *Q* and Q_c, with correction for depth: an essential aspect of modelling that is often ignored [1].

Table 2
Four hypothetical rock masses with reducing quality from top to bottom of the tabulation. Note the difference between *Q* and Q_c due to normalization by $\sigma_c/100$. Fig. 1 explains the derivation of E_m and conversion of the site-investigation V_P range to Q_c and thence to *Q*-value ranges.

RQD	*Jn*	*Jr*	*Ja*	*Jw*	*SRF*	*Q*	σ_c	Q_c	*FC*	*CC* (≈ MPa)	V_P (km/s)	E_m (GPa)
100	2	2	1	1	1	100	100	100	63°	50	5.5	46
90	9	1	1	1	1	10	100	10	45°	10	4.5	22
60	12	1.5	2	0.66	1	2.5	50	1.2	26°	2.5	3.6	11
30	15	1	4	0.66	2.5	0.13	33	0.04	9°	0.3	2.1	3.5

Please cite this article as: Barton N, Pandey SK. Numerical modelling of two stoping methods in two Indian mines using degradation of *c* and mobilization of φ based on *Q*-parameters. Int J Rock Mech Mining Sci (2011), doi:10.1016/j.ijrmms.2011.07.002

estimates have the advantage of not requiring software for their calculation—they already exist in the Q-parameter logging data, and the effect of changed conditions on parameters can be visualized easily. The new parameters *CC* and *FC*, hiding in the Q_c formula, are defined as below

'Cohesive component' $CC = (RQD/J_n)(1/SRF)(\sigma_c/100)$

'Frictional component' $FC = \tan^{-1}[(J_r/J_a)J_w]$

Note that all Q-parameter ratings in Ref. [3] were developed from trial-and-error fit to required rock bolt needs (bolting is compensation for low frictional strength?) and shotcrete needs (shotcrete is compensation for low cohesive strength?) for numerous tunnels and caverns spanning an order of magnitude of dimensions (3–30 m), and four orders of magnitude of rock quality (0.001–10). The fact that Q_c strongly resembles $c \times \tan\varphi$ (not $c+\tan\varphi$) perhaps emphasizes the inherent utility of this number as a multiple-orders-of-magnitude descriptor of rock mass conditions. The simple peak c and peak φ estimates have clear limitations, but they are *transparent*, and can be rejected if considered unrealistic. They will be used anyway in a presently quite unconventional manner. Note that some of the cohesion estimates far exceed the ultra-conservative RMR estimates of c and φ of some years vintage. This is a necessary improvement.

The P-wave velocity and (pseudo-static) deformation modulus estimates given in Table 2 are from the central diagonal, near-surface (nominal 25 m depth) inter-relationships given in Fig. 1. At greater depth both will be larger, even for the same Q-values.

There may be some other advantages of this simple semi-empirical approach, because the pairs of parameters RQD/J_n *and* J_r/J_a are already being logged at many mines, following the Potvin and Matthews method and the subsequent Modified Stability Graph, now in common use in Canadian and Australian mining for preliminary stope dimensioning. The original technique has been well documented in the literature, e.g. [4]. The method is based on a graph of the ratio of stope face area and perimeter (the 'hydraulic radius') to the rockmass stability number *N*, which is a direct product of the factors: RQD/J_n (block size) and J_r/J_a (frictional strength-or-weakness). Three other factors are added in the N' method, described by Hutchinson and Diederichs [5]. One of them is a stress term to allow for the strength-to-induced-stress ratio, as used prior to N' in estimating SRF. This addition is clearly needed in view of the frequent high stress environments. The mining industry appears to make frequent use of these stope design scoping methods, prior to eventual numerical modelling.

For the selection of appropriate modelling criteria, the mine-stope models to be reported here were first run using Mohr–Coulomb failure criteria and Hoek–Brown formulations, using strain softening properties [6], with a complete loss of cohesion and tensile strength, and significant loss of friction at around 0.07% of volumetric strain. The rock mass parameters were derived from Roclab™. These '$c+\tan\varphi$' models were followed by the '*c then* $\tan\varphi$' approach, with inspiration from the pioneering work described in Ref. [7] and discussed at length in Ref. [8], and referred to in Fig. 2. Their important findings, summarised in the next section, are a strong reason for our approach to the modelling of Zawar mining stopes, but the means of obtaining input data for the '*c then* $\tan\varphi$' approach are new, simple, and Q_c-based.

One point that needs to be addressed is the use of the factor SRF in calculating the basic Q value. The SRF value is raised to high values [9] when wishing to estimate approximate support needs for a single stress-fractured excavation in a previously massive rock mass with high RQD/J_n values. (The effective *RQD* is reduced in this EDZ when stress-fracturing occurs.) High values of *CC* will of course be relevant in such rock masses, prior to local tangential-stress-induced stress-fracturing when excavating. The extremely high SRF values that may be needed for selecting support of single highly stress-fractured excavations in what was originally a high RQD/J_n (massive) rock mass, should not be applied at the multi-stope modelling stage. As presently understood, and subject to experience gained in future application, we recommend using $SRF=5$ in a general 'high stress' situation, reserving the extreme SRF values, as previously, for individual excavation-support selection, in case of modelled or experienced intense local stress fracturing. This usually starts when the maximum tangential stress reaches about 0.4*UCS*, as shown in Barton and Grimstad's [10] Q-tables for *SRF* ratings, which 'take off' to high values beyond this stress/strength ratio.

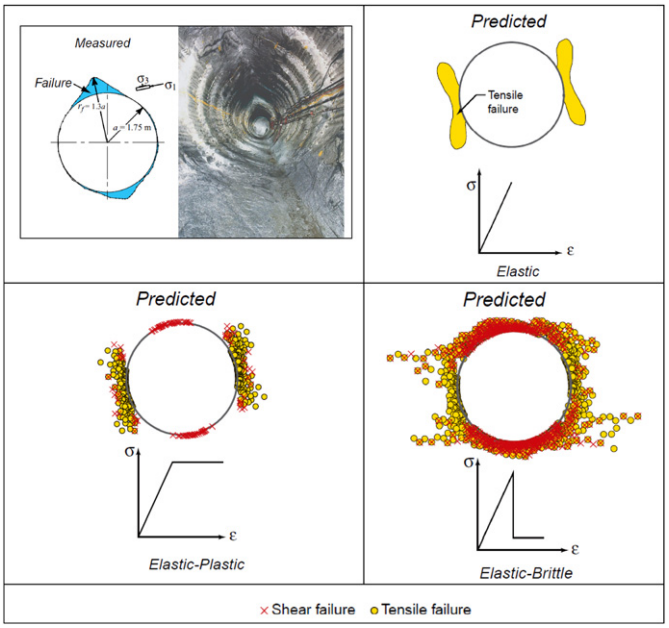

Fig. 2. Top left: The actual overbreak caused by a sub-horizontal major principal stress, as registered in the AECL/URL circular mine-by test tunnel, excavated by careful line drilling. Modelling of this simple geometry and rock mass was reportedly carried out using the Hoek–Brown failure criterion and the constitutive models suggested by Hoek and Brown [11]. The results from these models using the finite element programme Phase 2 are shown in the three remaining diagrams. Compared to the observed failure, none of the suggested modelling approaches predicted a failure zone that matched the shape of the observed V-shape notch. From Ref. [7], as also reported in Ref. [8].

3. Numerical continuum modelling shortcomings and solutions

The URL (Underground Research Laboratory) in Manitoba, Canada, was the site of numerous rock mechanics tests and novel *in situ* experiments. One of these was the excavation, by time-consuming but careful line drilling (not blasting), of a circular, mine-by experimental tunnel in a high stress environment. The authors Hajiabdolmajid et al. [7] reported that they used Hoek–Brown [11] rock mass strength formulations, and phase 2 FEM modelling to arrive at the highly unrealistic matches to reality shown in Fig. 2. This is surely a wake-up call to the profession that we must be more careful when planning to use the classic Mohr–Coulomb or Hoek–Brown based '$c+\tan\varphi$' approach, and perhaps follow fracture mechanics principles such as in the code FRACOD, or various 'damage mechanics' approaches (see various references in Ref. [2]). We should at least seriously consider using the '*c then* $\tan\varphi$' (or cohesion weakening and friction mobilization) approach, if continuing to use continuum approximations, whether with linear or non-linear shear strength approximations.

Please cite this article as: Barton N, Pandey SK. Numerical modelling of two stoping methods in two Indian mines using degradation of *c* and mobilization of φ based on Q-parameters. Int J Rock Mech Mining Sci (2011), doi:10.1016/j.ijrmms.2011.07.002

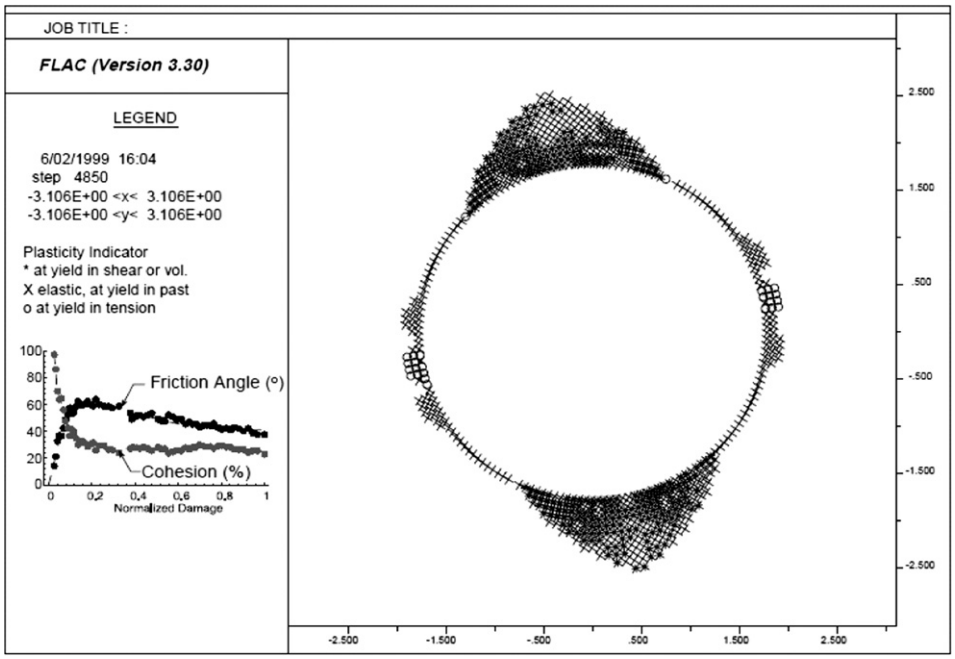

Fig. 3. The more logical "brittle cohesion-friction model" introduced by Ref. [7], that matches reality (Fig. 2: top-left) rather well. Note the degradation of cohesion and the mobilization, then slow degradation of friction. In the present modelling reported in this paper we suggest the validity of mobilizing and degrading friction in a more delayed manner, having regard for the proportion of jointing compared to intact rock, in the volume involved in eventual stress-induced failure.

Conventional continuum modelling of this class of problems is based on the assumption that the mobilization of the cohesion and frictional strength components is simultaneous. As emphasised in Ref. [8], this approach overlooks a fundamental observation of brittle failure, namely that the formation of tensile cracks (or log-spiral shear cracks as clearly seen in some TBM tunnels) may be the first step in the failure process. The model introduced in Ref. [7], shown in Fig. 3, implicitly captures some of the phenomena discussed earlier, by making cohesion weakening and friction hardening a function of plastic strain.

The cohesion softening and friction hardening (CSFH) model shown in Fig. 3 was implemented by the above authors in *FLAC* using its internal *FISH* language. As noted in the inset to this figure, the frictional strength (φ) after mobilization to a post-fracturing peak value was gradually reduced towards a 'residual' value. A material model with cohesion-softening and friction-hardening (CSFH) behaviour was also used in Ref. [12], in this case using the programme Phase 2, but also using Hoek–Brown GSI-based input data. Modelling results were compared with observed fallouts in six highly stressed excavations in Sweden and Norway, with good comparison in three of the reported cases. Mesh-size sensitivity and the shear strain sensitivity of shear-band development were also explored.

In the present study we have elected to test the application of a simpler approach to input data collection, using the *Q*-values logged in two mines in India, and have utilized the 'separate halves' of the Q_c formulation (*CC* and *FC*) as potential sources of peak cohesive and frictional strength. These values are, respectively, softened or mobilized to peak frictional strength and reduced towards residual. We also compare a conventional 'c plus tan φ' modelling approach to the 'c then tan φ' (or cohesion-softening and friction-hardening) modelling, and also compare modelled deformations with those recorded with pre-installed MPBX. Further we have the possibility of evaluating the validity of the input data (*Q*-based) through a competence factor based empirical approximation for deformation, based on *Q*, *UCS* and stress level. Clearly this is so far a little researched approach, but its validity seems to be clear from the results that we achieve, with the independent deformation recordings.

4. Mines of Zawar group and regional geology

The Zawar Group of Mines is the oldest lead–zinc mining area in India and is the location of an ancient heritage of mining and smelting operations. Ancient operations at Zawar date back to more than 2000 years. The extent of these operations is reflected by numerous ancient mine workings and smelting furnaces, in a well-preserved reflection of a civilization engaged in the business of mining and smelting of zinc. The Zawar Group comprising of four operating mines (Mochia, Balaria, Zawarmala and Baroi) has a cumulative production capacity of 1.2 Mtpa, along with an integrated and matching capacity for centralized mineral concentration and processing plants.

Both the Zawarmala Mine and the CW-0 lens of West Mochia mine of Hindustan Zinc Ltd., have host, and surrounding rock mass, consisting of metamorphosed dolomites belonging to the Aravalli super group of Pre Cambrian age, and they overlie the banded gneissic complex.

5. Methodology of present *Q*-based approach

The following two empirical equations for estimating the horizontal deformation in the walls and vertical deformation in the arch of a tunnel or cavern, or in a mining sense at the pillars and at the back of an opening, were introduced in Ref. [1]

$$\Delta v = SPAN(\sigma_V/\sigma_c)^{0.5}/100Q \quad (1)$$

$$\Delta H = HEIGHT(\sigma_H/\sigma_c)^{0.5}/100Q \quad (2)$$

An advantage of using these equations is that one can easily check the strains modelled numerically, with those recorded by the pre-mining-installed extensometers, to help indicate the approximate *Q*-value at a particular location. This approach therefore has inherent strength in checking the relevance of the results, thereby significantly reducing the uncertainties in modelling.

Please cite this article as: Barton N, Pandey SK. Numerical modelling of two stoping methods in two Indian mines using degradation of c and mobilization of φ based on *Q*-parameters. Int J Rock Mech Mining Sci (2011), doi:10.1016/j.ijrmms.2011.07.002

As detailed earlier, further correlations were introduced in Ref. [1] integrating V_P, Q, σ_c, depth, porosity and static deformation modulus E_m, and also for estimating the 'frictional and cohesive components' of the rock mass, in case of attempts to model this as a 'continuum'. The frictional component for a rock mass was defined as

$$FC = \tan^{-1}[(J_r/J_a)J_w] \quad (3)$$

The cohesive component was defined as

$$CC = (RQD/J_n)(1/SRF)(\sigma_c/100) \quad (4)$$

The above semi-empirical equations, in addition to other equations given below, were used in determining the input parameters for modelling the mines with Flac 3D.

The important point to be emphasized again is that the failure mode involved in rockmass breakage is highly unlikely to be governed by the Mohr–Coulomb or Hoek–Brown style of strength criterion '$c+\tan\varphi$', because rock fails at a small strain, breaking the cohesion, followed by mobilization of friction at a larger strain. We have therefore also used the '*c then* tan φ' approach, termed cohesion weakening and friction hardening in Ref. [7]. This is deliberately exaggerated with the present terminology '*c then* tan φ', to emphasise that traditional '*c plus* tan φ' thinking in rock mechanics needs selective revision (where significant stress fracturing may occur during shear failure).

5.1. In situ stress

The horizontal stress regimes at the Zawar Group of Mines are approximately as follows:

$\sigma_H = 0.048H + 4.4$ MPa; N−S, (perpendicular to strike)

$\sigma_h = 0.024$H$+2.2$ MPa; E−W, (parallel to strike)

where H is the depth below the surface in metres.

5.2. CW-0 lens

The first modelling objective is the CW-0 lens at West Mochia mine, which is being mined by the longitudinal *sub-level open stoping* method. The host rock is dolomite varying from pure dolomite through siliceous dolomite to arkosic dolomite. The mineralization is mostly in the pure dolomite, and this host rock has a compressive strength of approximately 120 MPa. The ore body has sub vertical dip and plunges in a westerly direction (Fig. 4).

The width of this ore body is quite small at around 25 m, but it has a strike length of approximately 300 m. The stopes are 85 m in strike with intervening rib pillars of 25 m width.

5.3. Determination of input parameters

The semi-empirical correlations used for estimating suitable input parameters were as follows:

$Q = (RQD/J_n)(J_r/J_a)(J_w/SRF)$, and $Qc = Q\sigma_c/100$

$E_{mass} = 10(Qc)^{1/3}$ GPa

Generalized Poisson's ratio $v = 0.25$

Bulk modulus $= E/3(1-2v)$(GPa)

Shear modulus $= E/2(1+v)$(GPa)

FC = Frictional component $= \tan^{-1}[(J_r/J_a)^*J_w]$

CC = Cohesion component $= (RQD/J_n)(1/SRF)(s_c/100)$ (MPa)

Tensile strength $\approx c/\tan(FC)$ (MPa)

Using the above correlations and approximations, the input parameters determined from Q-logging of various locations are summarized in Table 3.

The lens was modelled first using the '*c plus* tan φ' approach and then with the '*c then* tan φ' approach. The contrast between the two approaches to cohesion degradation and frictional

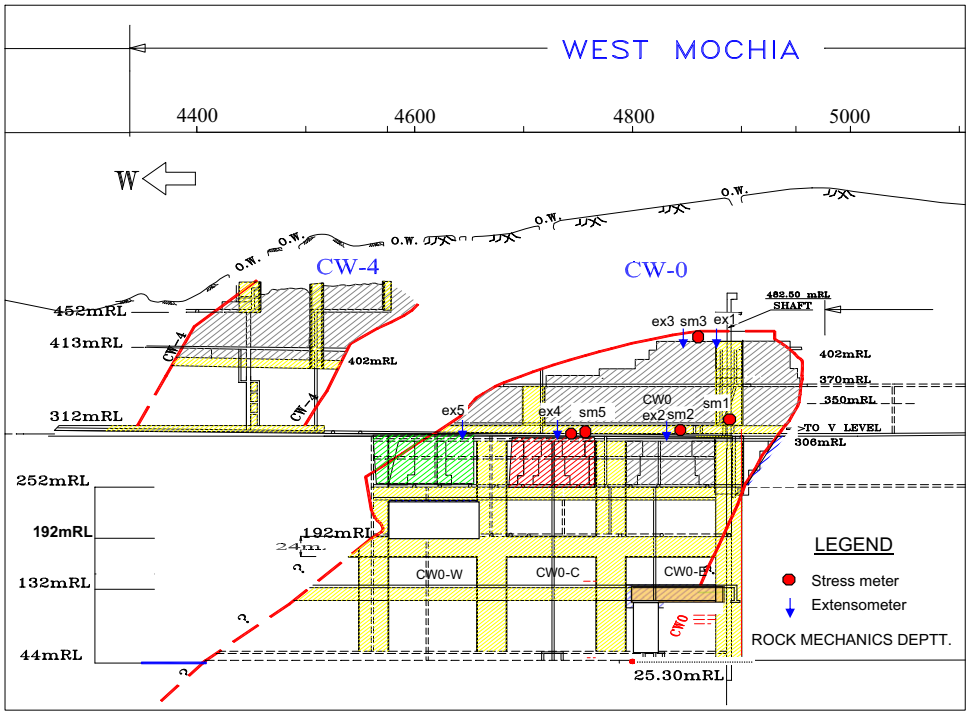

Fig. 4. Longitudinal vertical section of the West Mochia Mine, showing the westerly plunging orebody.

Please cite this article as: Barton N, Pandey SK. Numerical modelling of two stoping methods in two Indian mines using degradation of c and mobilization of φ based on Q-parameters. Int J Rock Mech Mining Sci (2011), doi:10.1016/j.ijrmms.2011.07.002

ARTICLE IN PRESS

Table 3
The input parameters determined for the CW0-0 lens of West Mochia Mine. Note deliberate limitation of unrealistic decimal places. (mRL is the mean reduced level, roughly corresponding to mean sea level.)

Location/level (mRL)	Q	Q_c	E_{mass} (GPa)	Bulk modulus (GPa)	Shear modulus (GPa)	Cohesion (MPa)	Friction angle (deg.)	Tensile strength (MPa)
452	21	25	29.2	19.4	11.7	8.5	71.0	2.9
452–250	56	68	40.8	27.2	16.3	17	76.0	4.3

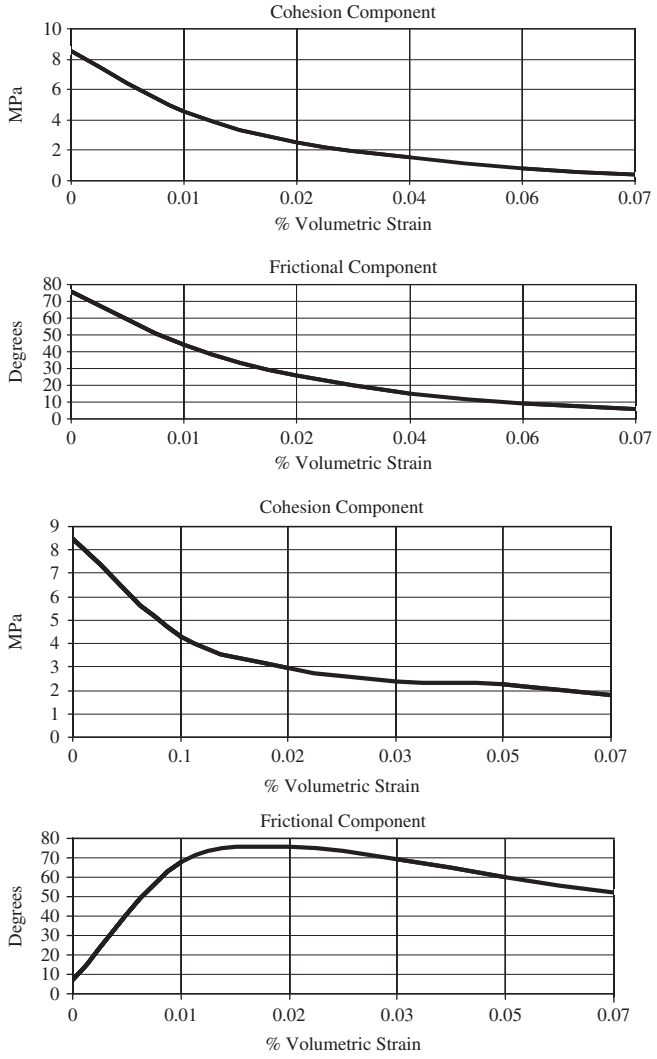

Fig. 5. Top two: the '$c+\tan\varphi$' approach. Bottom two: the 'c then $\tan\varphi$' approach.

mobilization is shown in Fig. 5. Concerning the apparently 'very high' peak friction angles, one should bear in mind that the intact rock portion of the failure surface may also exhibit (lab-scale) dilation angles ranging (at mining-relevant confining pressures) from about 5° to 45° depending on the strength of the rock type [13]. Rough joints and tension fractures in hard rock with high *JCS* dilate just as much [14]. In fact the mobilization and subsequent degradation of the 'intact rock' dilation angle during several % of plastic shear strain, very much resembles the mobilized roughness (JRC_{mob}) used to model the shear stress-deformation behaviour of joints and fractures, as used by Barton and Bandis, 1982 [15] in the BB model.

The lens CW-0 has been mined along the full strike from 447 to 324 mRL. Thereafter, a sill pillar of 15 m from 324 to 309 mRL (306 mRL being the bottom of the drive), is left in situ. Below 306 mRL, the lens has been divided into three parts namely CW-0: E, C and W. The lens has been depicted in Fig. 5 as mined up to CW-0 (C). At present, mining is underway at CW-0 (W).

Table 4
Comparison of results from two approaches to modelling explained: Figs. 7–14.

Component	$c+\tan\varphi$	c *then* $\tan\varphi$
Maximum stresses	Stresses are concentrated in the crown pillar above CW-0 (E) and CW-0 (C), with less stress transfer through the rib pillar between the stopes. (See Fig. 6).	Stresses are concentrated above CW-0 (E) only, with transfer of stress along the rib pillar. (See Fig. 7).
Minimum stresses	Tensile stresses are not distributed evenly along the periphery of the stopes. (See Fig. 8).	Immediate stope periphery rocks experience tensile stresses in all the stopes. (See Fig. 9).
Shear stresses	No concentration of shear stresses in the back (roof) of the stopes. (See Fig. 10).	Concentration of shear stresses above the stopes, and development of an 'internal' shear band. (See Fig. 11).
Z-displacement	Maximum strains are concentrated at the back of the stope at 447 mRL at the maximum height. The magnitudes are less between 358 and 447 mRL. (See Fig. 12).	Continuous zone showing similar strains all along the back of the stope between 358 and 447 mRLs. (See Fig. 13).

6. Comparison between the two modelling approaches

The principal differences between the results of the two modelling approaches are summarized in Table 4, with reference to the relevant figures in each case. Figs. 6–13 follow in sequence and without additional text.

6.1. Model calibration

The model output with respect to strains is used for the calibration or checking of the results, which is possible because MPBX were installed prior to mining of the stopes, and we are also able to utilize the Q-based empirical model for predicting expected displacements.

6.1.1. Estimated vertical movement at the back of the stope at 447 mRL using Eq. (1)

Span = 85 m, $Q=56$, $\sigma_V \approx 3.6$ MPa (for 123 m of overburden), $\sigma_C = 120$ MPa

$$\Delta V = SPAN(\sigma_V/\sigma_C)^{0.5}/100Q = (85000/5600)\sqrt{(3.6/120)} = 2.6\,\text{mm}.$$

The MPBX at the location is inclined at $\approx 50°$. The acting anchor has recorded a total deformation of 3.48 mm. The vertical deformation of the back of the stope would be $\sin 50° \times 3.48 = 2.7$ mm (see Fig. 13).

Please cite this article as: Barton N, Pandey SK. Numerical modelling of two stoping methods in two Indian mines using degradation of c and mobilization of φ based on Q-parameters. Int J Rock Mech Mining Sci (2011), doi:10.1016/j.ijrmms.2011.07.002

6

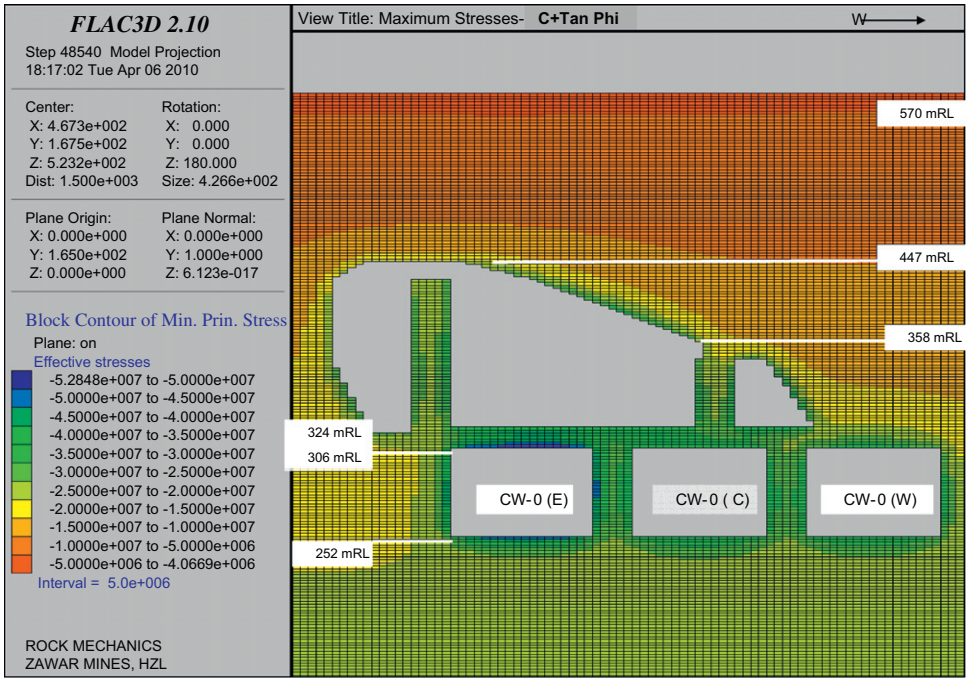

7

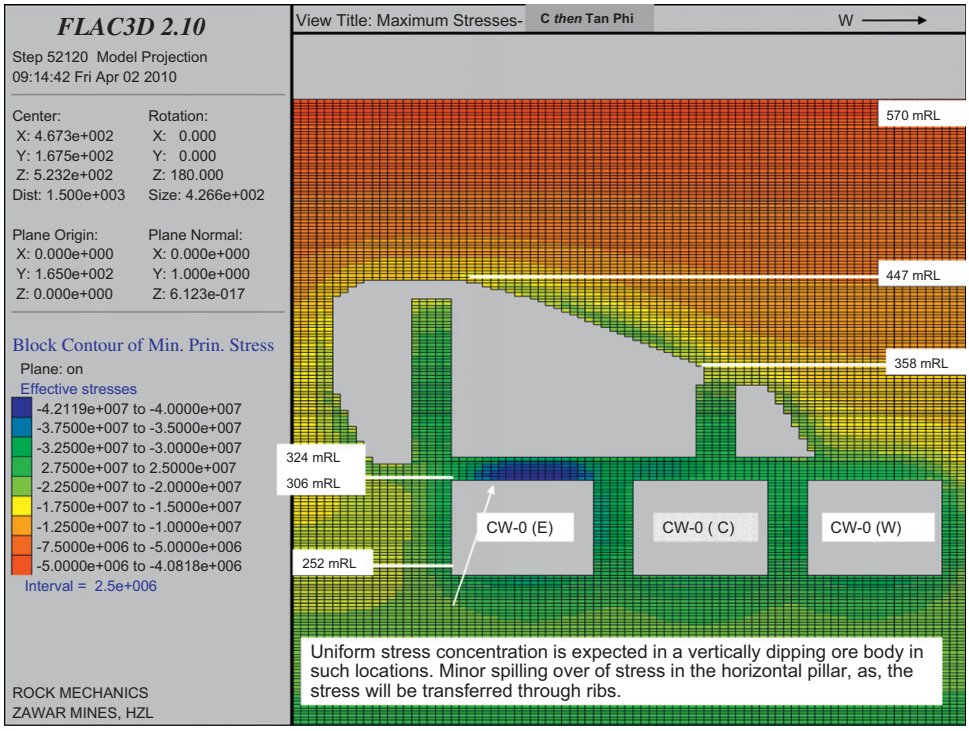

Figs. 6 and 7. Principal maximum stresses in N–S direction, perpendicular to the plane of observation. Top figure shows conventional '$c+\tan\varphi$' approach, bottom figure shows unconventional 'c then $\tan\varphi$' approach.

6.1.2. Estimated vertical movement at the back of the CW-0 (C) stope using Eq. (1)

Span=85 m, Q=56, σ_V=6.6 MPa (for 230 m of overburden), σ_C=120 MPa.

$$\Delta V = SPAN(\sigma_V/\sigma_C)^{0.5}/100Q = (8500/5600)\sqrt{(6.6/120)} = 3.5\,\text{mm}$$

The MPBX installed at the back of the stope recorded a total deformation of 4.52 mm during the mining of CW-0 (C) stope and a total deformation of 4.78 mm up to the present, after the mining of CW-0 (W) (Fig. 13). Since the MPBX is installed at an angle of 52°, the actual vertical movement at the stope back would be $\sin 52^\circ \times 4.52 = 3.56$ mm, and $\sin 52^\circ \times 4.78 = 3.76$ mm (see Fig. 13).

Similarly, for CW-0 (E), the calculated movement at the back of the stope comes to 1.24 mm. The model predicts 1–2 mm (Fig. 13). The model also predicts similar deformation magnitudes at the locations of the MPBX, whose deformation-time trends are shown in Figs. 14 and 15.

Please cite this article as: Barton N, Pandey SK. Numerical modelling of two stoping methods in two Indian mines using degradation of c and mobilization of φ based on Q-parameters. Int J Rock Mech Mining Sci (2011), doi:10.1016/j.ijrmms.2011.07.002

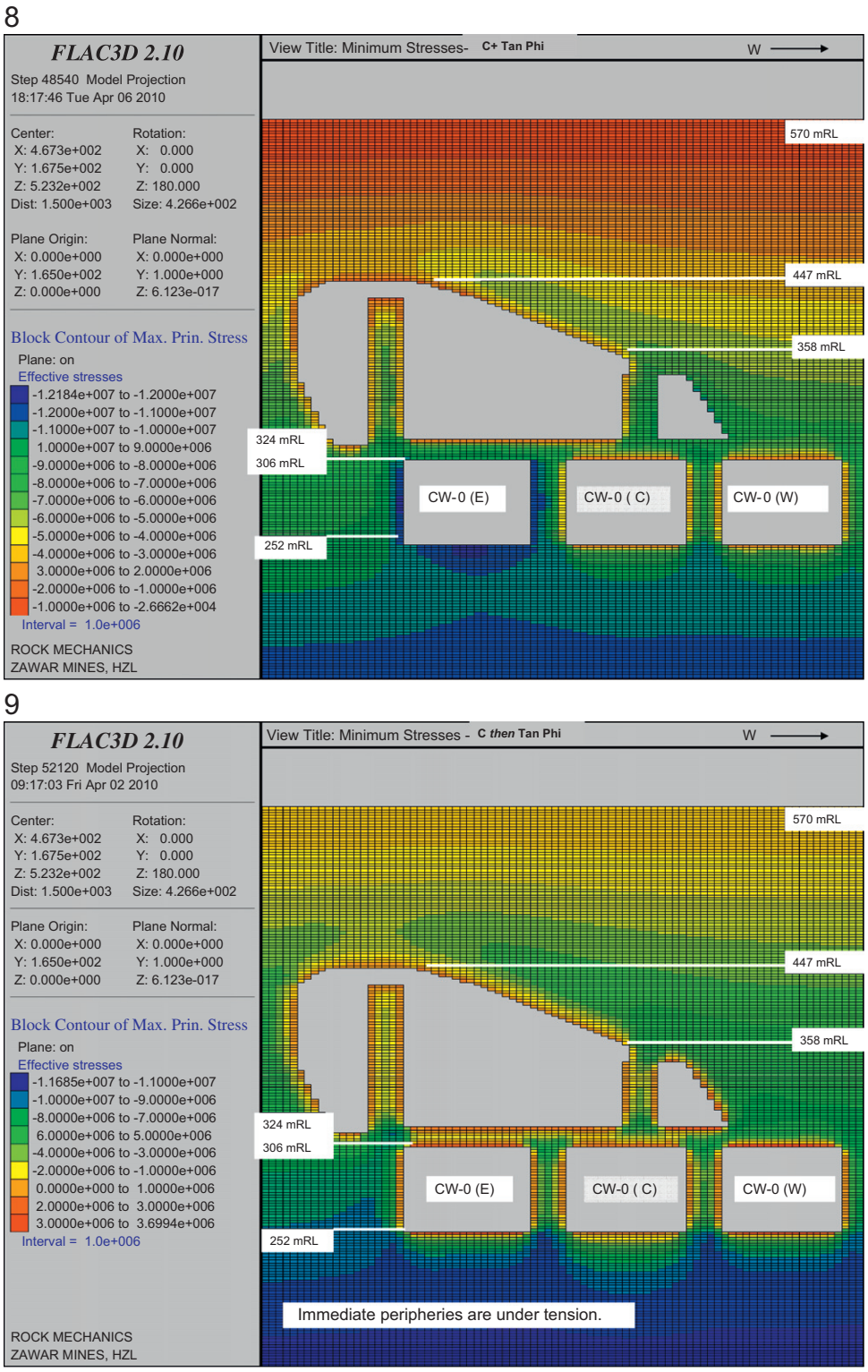

Figs. 8 and 9. Principal minimum stresses parallel to the plane of observation. Top figure shows conventional '$c+\tan\varphi$' approach, bottom figure shows unconventional 'c then $\tan\varphi$' approach.

7. Zawarmala mine

At the second mine to be analysed, mineralization is concentrated at the core of an anticline and follows the axial plane of the fold plunging 40° due North. The host rock is dolomite varying from pure dolomite through siliceous dolomite to arkosic dolomite. The mineralization is mostly in pure dolomite, again having a compressive strength of 120 MPa. The mine practices transverse sub-level open stoping without backfilling. The typical mining geometry is 24 m wide stopes with 14 m wide intervening rib pillars. The ore is mined for the full height and as a result, the stopes are higher as one moves down the plunge. Two sill pillars, one of 13 m thickness at 446 mRL and the other, 15 m thick at 355 mRL are left in situ. Another 20 m thick is proposed at

Please cite this article as: Barton N, Pandey SK. Numerical modelling of two stoping methods in two Indian mines using degradation of c and mobilization of φ based on Q-parameters. Int J Rock Mech Mining Sci (2011), doi:10.1016/j.ijrmms.2011.07.002

10

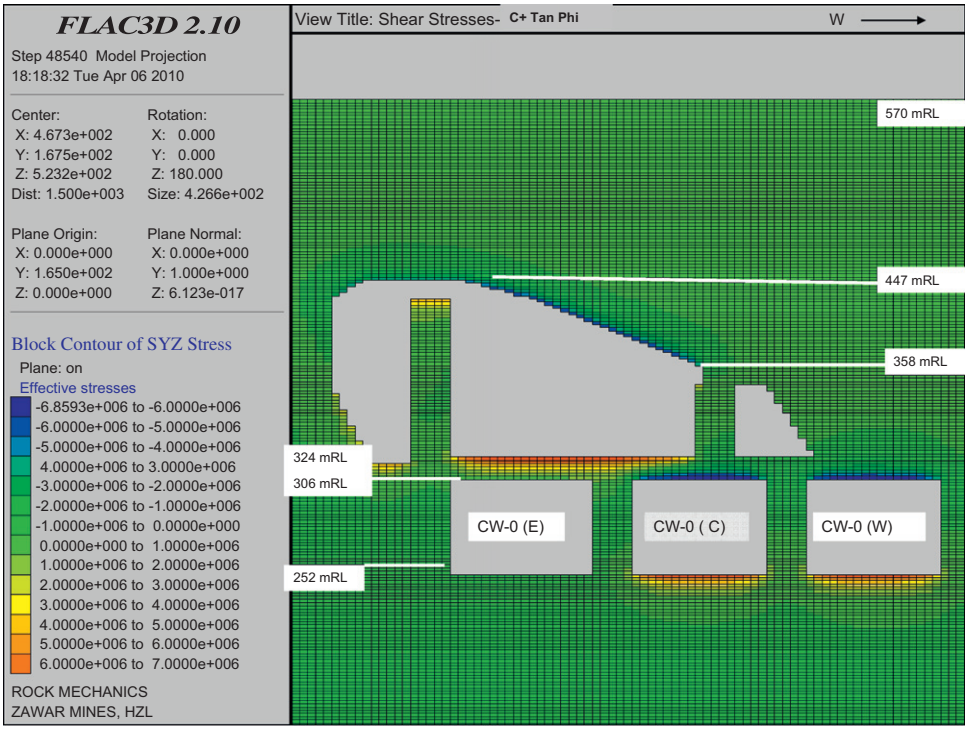

11

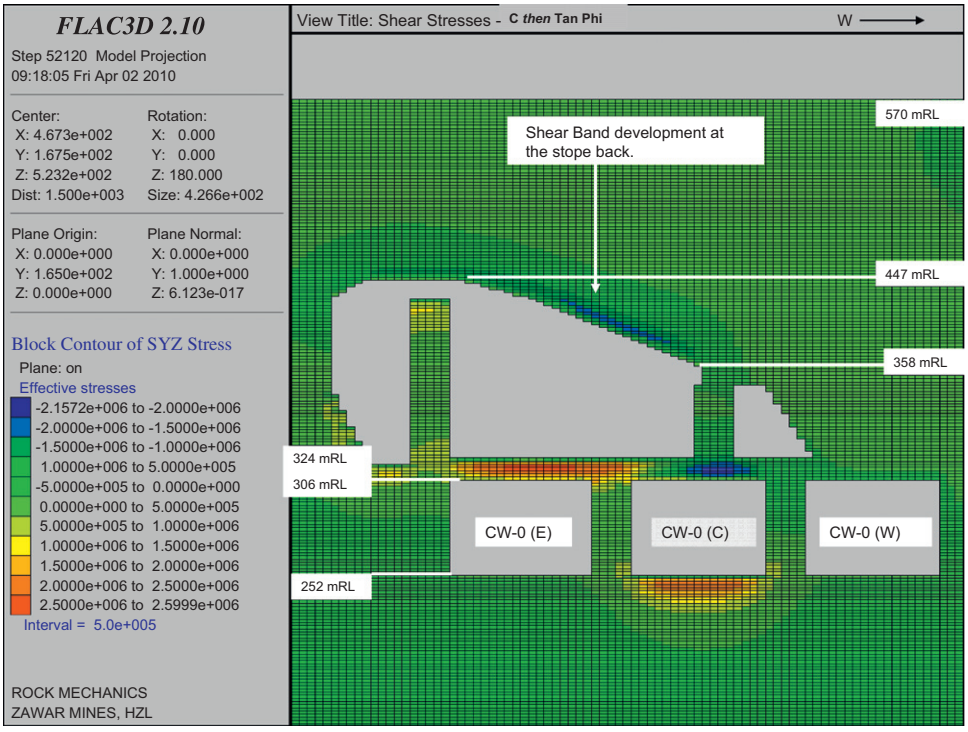

Figs. 10 and 11. Maximum shear stresses in the plane of observation. Top figure shows conventional '$c+\tan\varphi$' approach, bottom figure shows unconventional 'c then $\tan\varphi$' approach. Note the shear band development behind the stope back, in the 'c then $\tan\varphi$' model.

210 mRL. The geometry of the stopes is shown in vertical cross-section in Fig. 16a, and representation in FLAC3D in Fig. 16b.

7.1. Determination of input parameters

Scan line and at places, detailed geotechnical mapping was done to determine the rock mass quality Q at various working levels. The rock mass is massive with the joint frequency analyses showing up to 60% of joints having trace lengths of less than 50 cm. The joints are rough and undulating in general. The rock mass can be considered as well fractured but with high inter-block shear strengths, giving high J_r/J_a ratios. A typical joint survey for the mine is provided in Table 5.

Please cite this article as: Barton N, Pandey SK. Numerical modelling of two stoping methods in two Indian mines using degradation of c and mobilization of φ based on Q-parameters. Int J Rock Mech Mining Sci (2011), doi:10.1016/j.ijrmms.2011.07.002

12

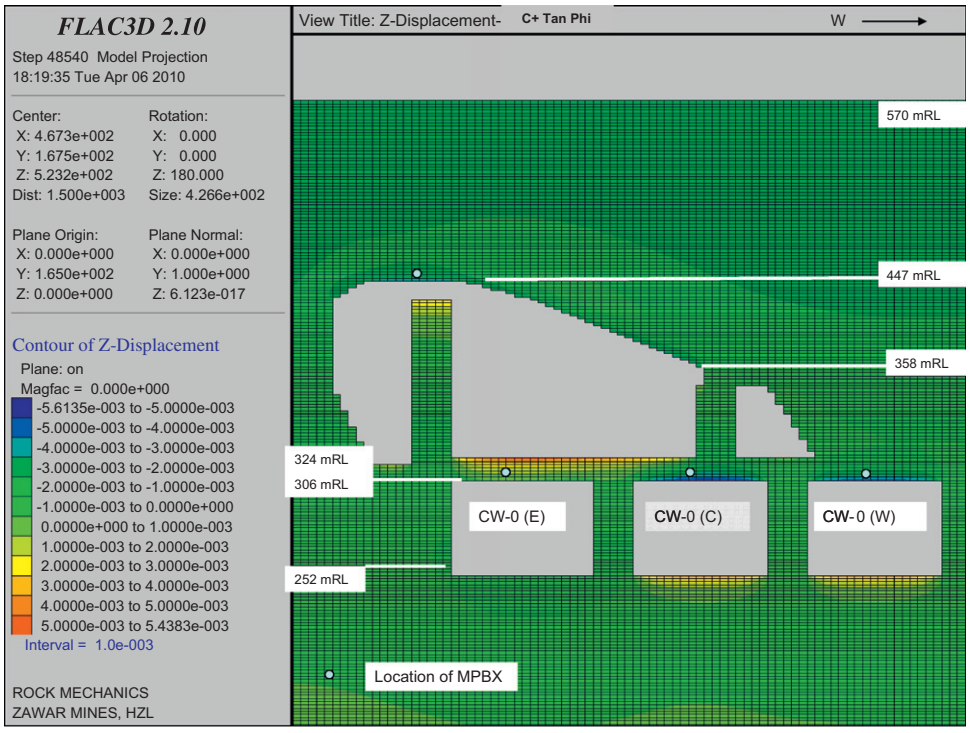

13

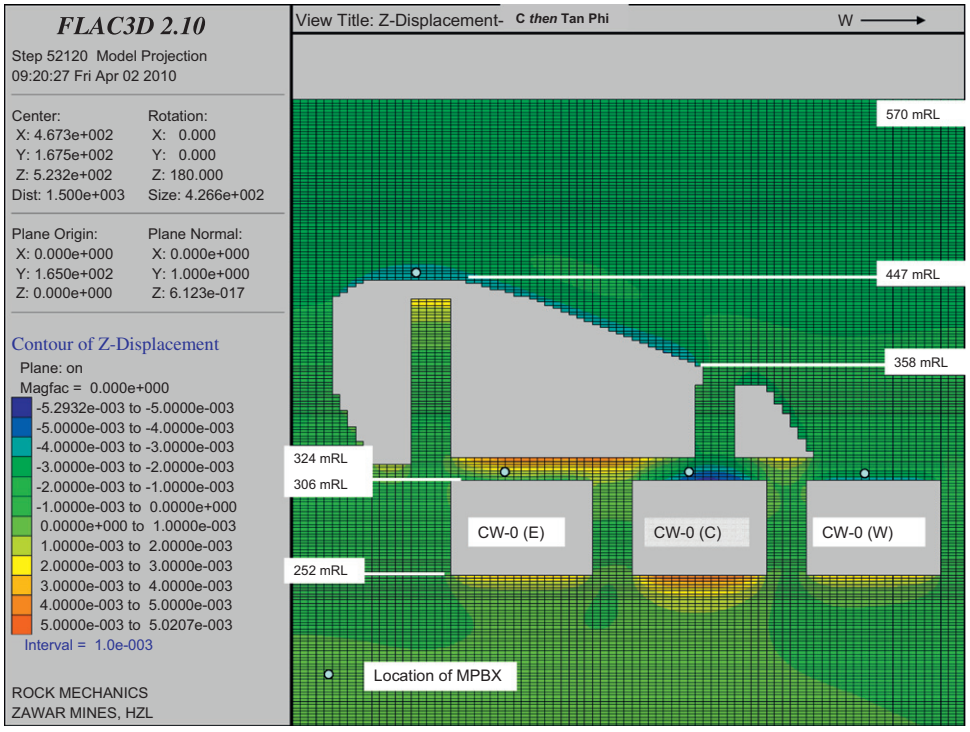

Figs. 12 and 13. Vertical *Z*-displacement component. Top figure shows conventional '$c+\tan\varphi$' approach, bottom figure shows unconventional 'c then $\tan\varphi$' approach. Note greater vertical closure caused by the behaviour of the 'skin' of the main stope.

Based on the equations described previously, the rock mass input parameters were estimated, and are summarized in Table 6. The model was run utilizing the '*c then* tan φ' approach.

7.2. Model calibration

The displacements at the back and the horizontal movements in the rib pillars and the MPBX trends are in good agreement. Eqs. (1) and (2) are used to calculate the likely movement at the back of the stopes and in the rib pillars.

7.2.1. Estimated vertical deformation of the back of S-4 stope at 338 mRL

Q at 338 mRL=38. Overburden=232 m (570–338 mRL), rock density 3.0 gm/cc, $\sigma_V \approx 7$ MPa, $\sigma_C = 120$ MPa, span=24 m,

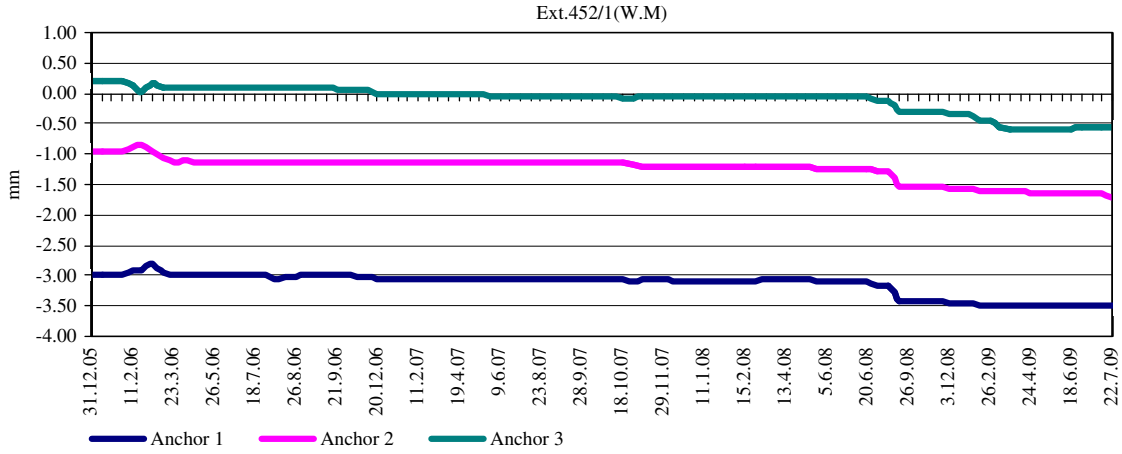

Fig. 14. Deformation-time trends for MPBX 452/1.

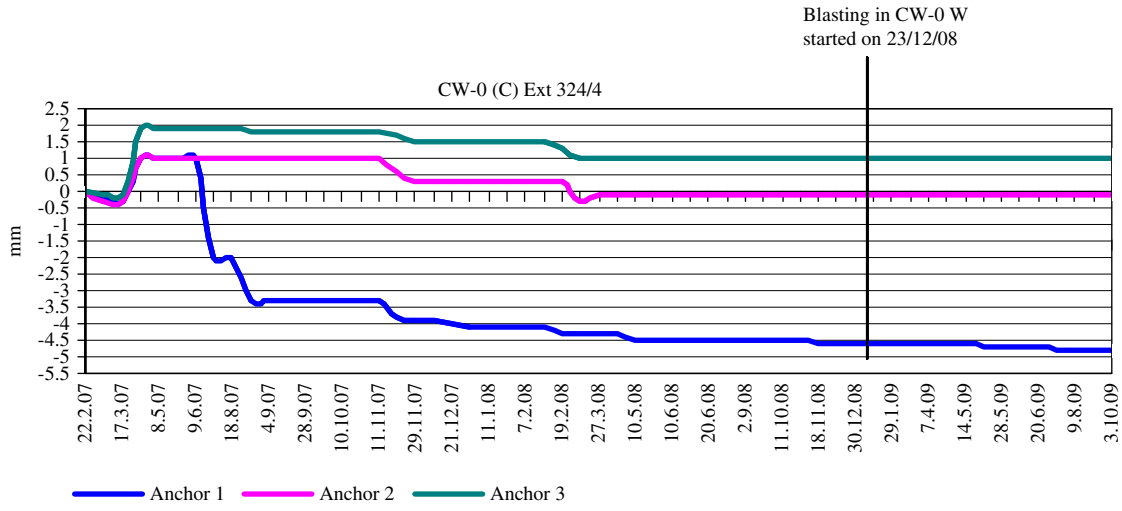

Fig. 15. Deformation-time trends for MPBX 324/4.

$\Delta V = (SPAN/100Q)(\sigma_V/\sigma_C)^{0.5} = (24{,}000/3800) \times 0.2415 = 1.5$ mm. The MPBX at the location recorded a total deformation of 2.19 mm. Since the MPBX is inclined at $\approx 45^\circ$, the actual vertical movement at the back of the stope $= \sin 45^\circ \times 2.19 = 1.55$ mm. The model predicts a deformation of 1.5 mm (see Figs. 17–19, location 3 and 4).

7.2.2. Estimated horizontal movement at 394 mRL for R-2 pillar between S-2 and S-3 stopes

Height of the pillar at 394 mRL = 28 m (S-2 Stope is from 433 to 366 mRL). The overburden = 176 m (570–394 mRL), $\sigma_H = 176 \times 0.048 + 4.4 = 12.9$ MPa. $\sigma_C = 120$ MPa, height = 28 m, $Q = 38$, ΔH (at 394 mRL) $= 28{,}000/(38 \times 100) \times (\sqrt{}12.9/120) = 2.4$ mm. The model shows 2–3 mm (see Fig. 17, location 1).

7.2.3. Estimated horizontal movement S-3 stope—433–355 mRL

The height of the pillar at 390 mRL is 39 m. ΔH (at 300 mRL) $= 39{,}000/(38 \times 100) \times \sqrt{}(12.85/120) = 3.4$ mm. The model shows 3.0–5.0 mm (see Fig. 17, location 2).

The above comparisons indicate that the model has been calibrated with the ground conditions to the best possible extent, and the closeness of the results and measurements seems to validate both the modelling and the depth-dependent estimates of deformation modulus, but of course this could be fortuitous.

7.3. Crown blast and its affect

In November 2005, the horizontal pillar between 335 and 338 mRL for S-3 stope was mass blasted. Initially there was no discernable change in the extensometer and the stress metre readings except a relaxation of 1.5 MPa. Such behaviour was expected and after the pillar started shedding some 'skin' mainly towards the S-3 stope, the stress metre started showing stress build-up.

In February 2006, two rings to recover the trough pillar in an adjacent stope L-4 were also blasted (see Fig. 16). The stress metre in the R-3 Pillar showed a build-up of 8 MPa in a seven month period indicating more and continuous shedding of the skin, resulting in the thinning of the pillar. At the same time a fault plane that was concealed earlier and dipping 73° due 225°, started showing displacement (Fig. 20). This is evident from the change in the velocity and the displacement vectors in the area. The two vectors that were at 120–130° earlier, point in the same direction, towards the S-3 stope, post blast (Figs. 21 and 22).

7.4. Effect of blasting of adjacent stopes

S-6 stope was almost complete at the time of the crown blast. The rate of movement along the fault plane was discernable until the time the S-7 stope was blasted. However, after the completion

Please cite this article as: Barton N, Pandey SK. Numerical modelling of two stoping methods in two Indian mines using degradation of c and mobilization of φ based on Q-parameters. Int J Rock Mech Mining Sci (2011), doi:10.1016/j.ijrmms.2011.07.002

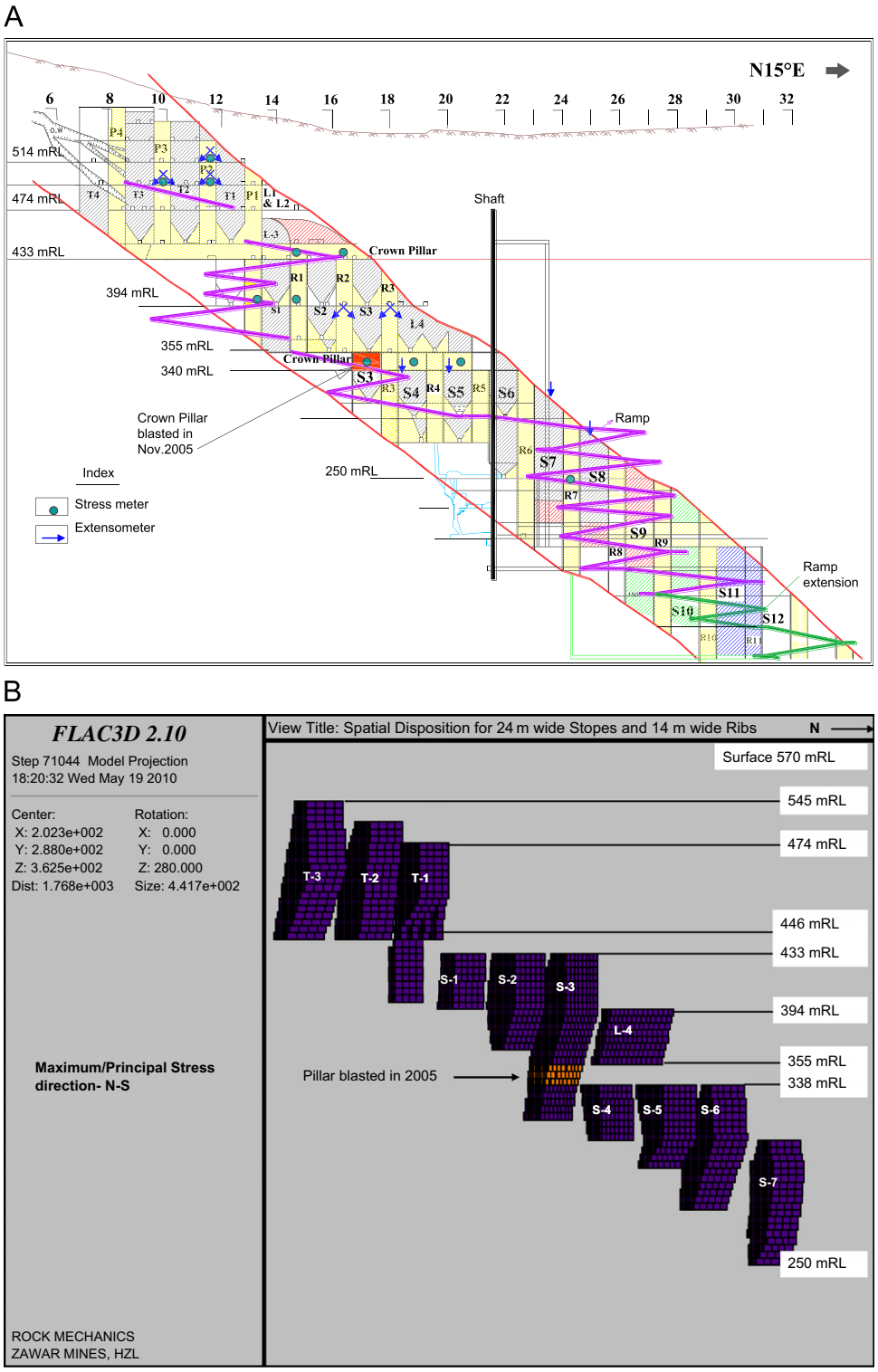

Fig. 16. Longitudinal vertical section and spatial disposition of stopes in the Zawarmala Mine. Note the 24 m width of stopes and the 14 m wide ribs between the stopes.

Table 5
Joint set descriptions in Zawarmala Mine.

Joint set	Dip	Dip direction	Spacing (cm)	Remarks
J1 (foliation)	20–45°	330°	20	
J2	50–70°	270–280°	20	Slight movement evident in places—shear joints (?)
J3	45–70°	145–200°	20	Discontinuous, trace lengths seldom exceed 1.5 m.
J4	68°	270°	10–15	Bedding joints

Please cite this article as: Barton N, Pandey SK. Numerical modelling of two stoping methods in two Indian mines using degradation of c and mobilization of φ based on Q-parameters. Int J Rock Mech Mining Sci (2011), doi:10.1016/j.ijrmms.2011.07.002

Table 6
Rock mass properties estimated for the Zawarmala mine, HZL.

Location/level (mRL)	Q	Q_c	E_m (GPa)	Bulk modulus (GPa)	Shear modulus (GPa)	Cohesion (CC) (MPa)	Friction angle (deg.)	Tensile strength (MPa)
500	20	24	28.8	19.2	11.5	8.8	71.6	2.7
430	21.3	25.5	29.4	19.6	11.8	8.5	71.6	2.8
355	38	45	35.6	23.7	14.2	11.3	76.0	2.8
250	53	63.6	39	26.6	15.9	12	79.4	2.3

(mRL roughly corresponds to mean sea level).

17

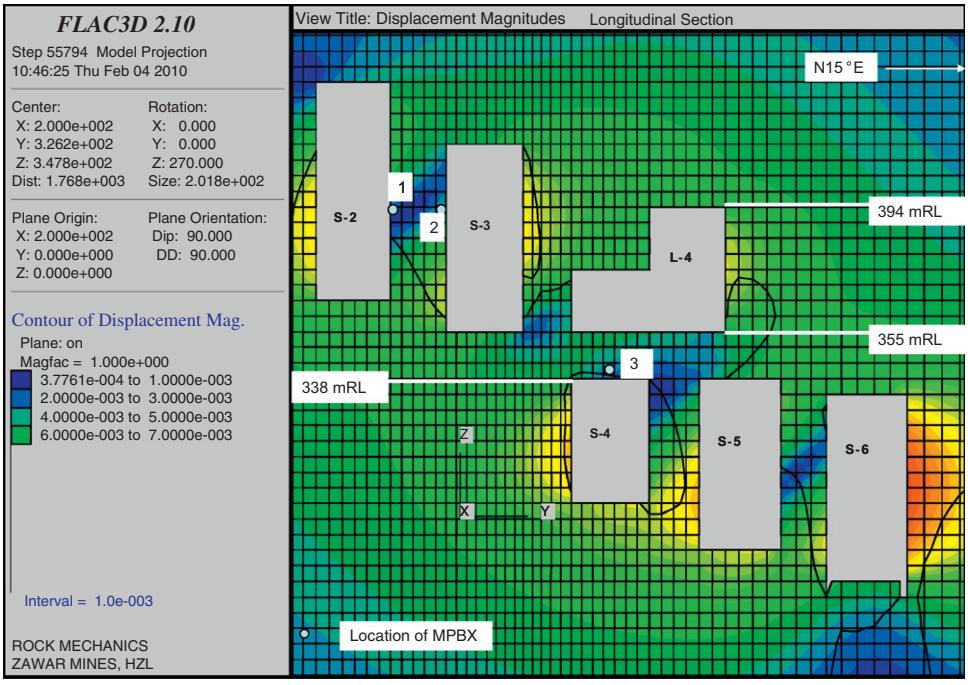

18

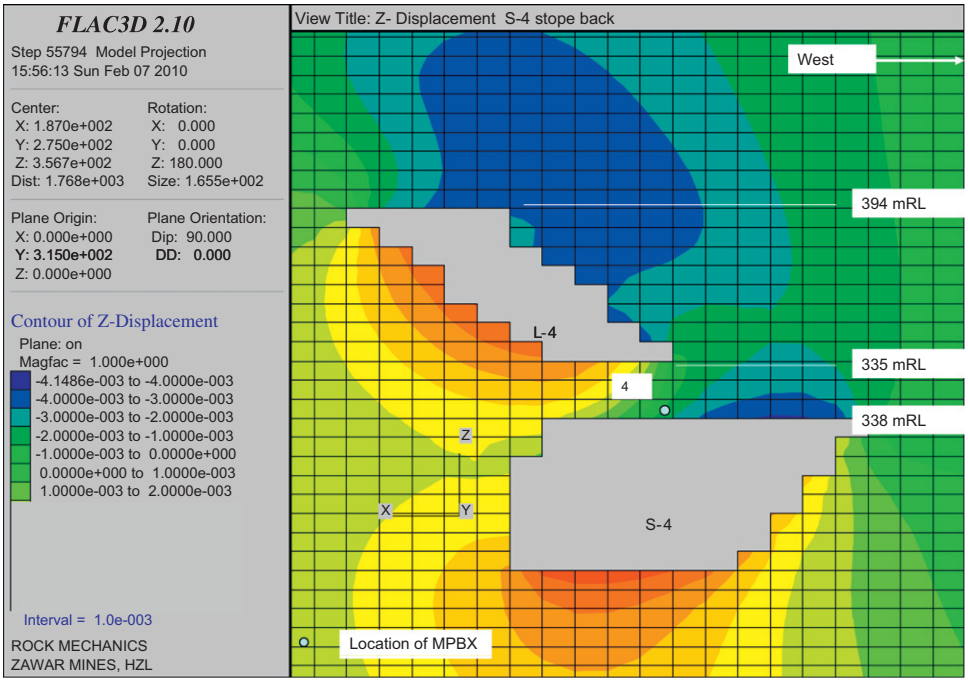

Figs. 17 and 18. Displacement magnitudes and vertical displacement at the stope back. Note the location numbers # 1 to #4 used in the previous model-calibration section.

Please cite this article as: Barton N, Pandey SK. Numerical modelling of two stoping methods in two Indian mines using degradation of c and mobilization of φ based on Q-parameters. Int J Rock Mech Mining Sci (2011), doi:10.1016/j.ijrmms.2011.07.002

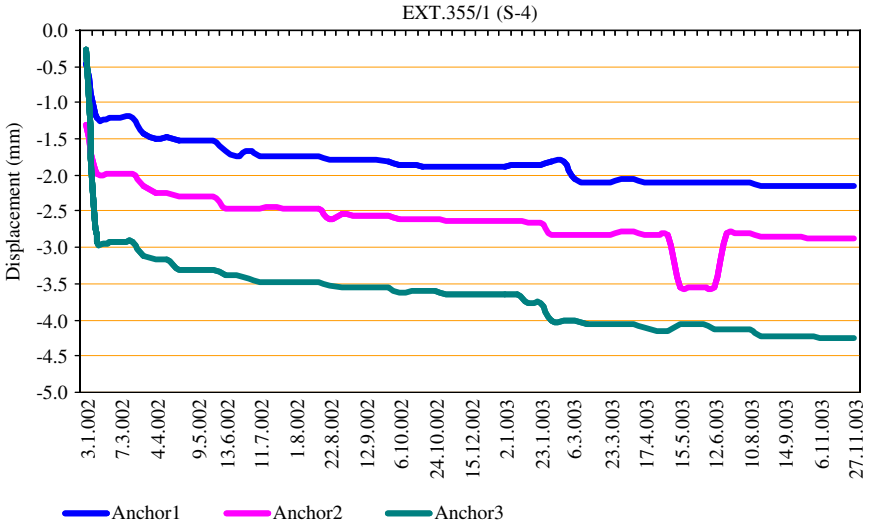

Fig. 19. MPBX extensometer 335 that was installed pre-mining.

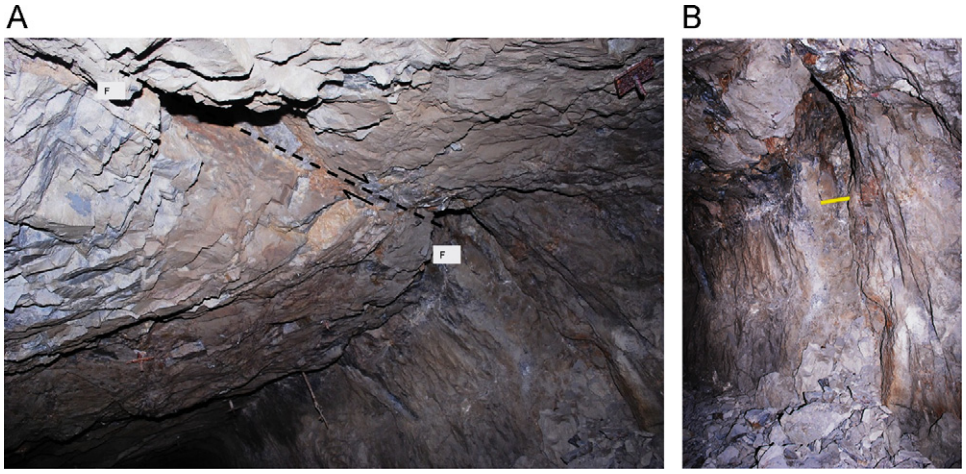

Fig. 20. Two views of the fault plane that started to show shear displacement.

of S-7 stope, the rate of movement along the fault decreased considerably. This is evidently supported by the direction of the modelled velocity vectors in the area (see Fig. 23)

Another aspect worth mentioning is the increase in the 'zone under tension' in rib pillars. This zone, which is insignificant in the rib pillars in the upper horizons, nevertheless increases significantly as the mining progresses with depth. Since the rock mass is susceptible to ground vibrations under low confinement, spalling of the pillar sides is accentuated with blasting of adjacent stopes, thereby further reducing the effective width of the pillars and ultimately their load bearing capacity.

7.5. Modelling input using HB parameters

The Zawarmala mine was subsequently modelled using the parameters arrived at using Roclab™. In attempting this modelling the following aspects needed consideration, because first attempts were made to model using the recommended $GSI=RMR-5$, but this did not give workable results as the model showed failure in one form or the other.

Because of the above instability, and because of the relationship between these quality numbers is approximate anyway, a less conservative $GSI=RMR$ assumption was made, meaning a larger *GSI* input value. Furthermore, *RMR* was calculated using the approximation $RMR=50+15\log Q$ [1], since RMR logging was not used at the mine. There are then two further parameters that need special mention: (a) the rock disturbance factor, *D*; two different values were assumed and (b) the tensile strength (a too low value is suspected: see below). At a depth of 118 m, $\sigma_3=3.4$ MPa, $\sigma_{ci}=120$ MPa, $GSI=71$, $m_i=20$, and $E_i=45$ GPa.

The rock mass properties arrived at for different *D* values were as given in Table 7.

7.6. Modelling results

Using the above two different sets of parameters, the models failed. The reasons could be: (a) low E_{rm}, for $D=0.4$, or (b) low tensile strength. However, after estimating the tensile strength from $c/\tan\varphi$, the model did give results for $D=0$.

Various attempts to model this mine using HB parameters failed in one form or another. In some cases the model failed through the development of conjugate sets of fractures and in others through the development of a fracture plane at different locations in the rock mass. Changes in modelling methodology also did not give any result. Since the mine exists and is not failing, except in very minor over-stressed locations as is normal, then something fundamentally seems to be wrong with one or more of the input parameters.

Please cite this article as: Barton N, Pandey SK. Numerical modelling of two stoping methods in two Indian mines using degradation of *c* and mobilization of φ based on *Q*-parameters. Int J Rock Mech Mining Sci (2011), doi:10.1016/j.ijrmms.2011.07.002

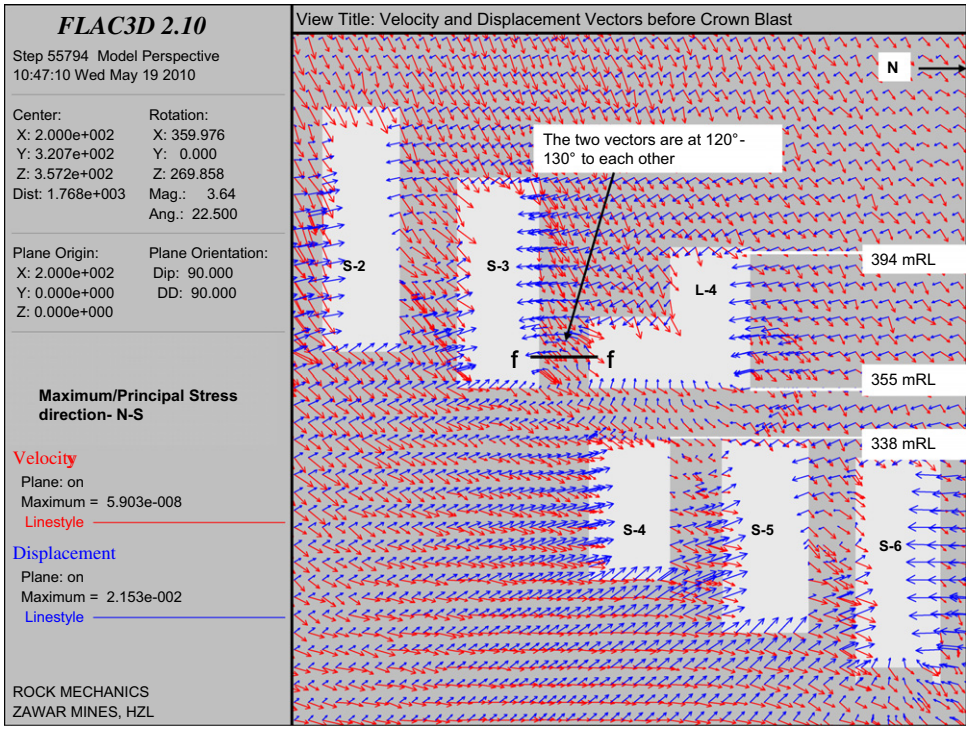

Fig. 21. Velocity and displacement vectors at the fault plane location that started to show shear displacement—before crown blast.

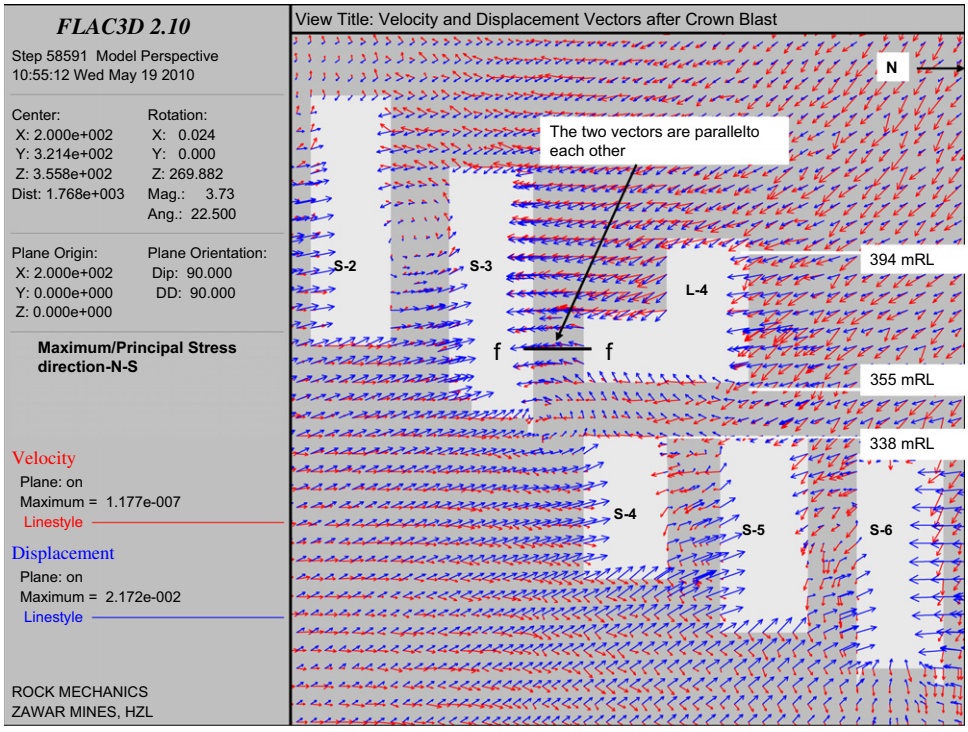

Fig. 22. Velocity and displacement vectors at the fault plane location that started to show shear displacement—after crown blast.

8. Difference between the two modelling approaches

The initial response of the rock mass to an excavation is governed by its modulus of elasticity or in other words, by the bulk and shear modulus. As depths increase, and stress levels increase, rock masses with low bulk and shear moduli will suffer more displacement, and for a given (low enough) shear modulus, the rock mass may fail with the development of shear fractures. This type of behaviour is accentuated if the cohesion and the friction values are low.

Please cite this article as: Barton N, Pandey SK. Numerical modelling of two stoping methods in two Indian mines using degradation of c and mobilization of φ based on Q-parameters. Int J Rock Mech Mining Sci (2011), doi:10.1016/j.ijrmms.2011.07.002

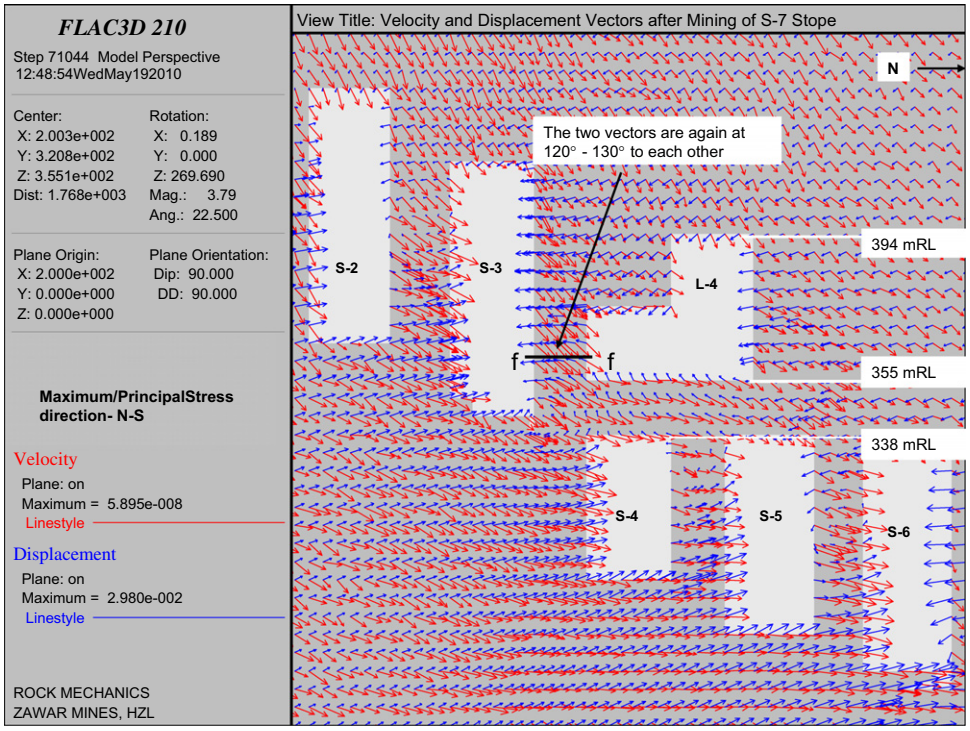

Fig. 23. Modelled deformation vectors after the crown blast, and after the S-7 stope mining, compared to the prior condition.

Table 7
Variation in rock mass properties for different 'Rock Disturbance Factor' D values. (Note the deliberate deletion of decimal places, far different from the eight decimal places sometimes published by those using such methods).

Property	$D=0$	$D=0.4$
Cohesion (MPa)	3.3	2.8
Friction angle (deg.)	58.5	56.9
Tensile strength (MPa)	−0.7	−0.5
E_{rm} (GPa)	33.8	22.9

Table 8
Roclab™ use of Hoek–Brown formulations showing varied (non-linear) c and φ with depth, but constant E_{rm}. Note that some rounding of decimal places has been made: much more would be justified in view of the obvious uncertainties in all rock mechanics input data, by whatever method.

Depth (m)	100	200	400	500
σ_3 (MPa)	2.94	5.88	11.77	14.71
Cohesion (MPa)	3.15	4.08	5.76	6.53
Friction (deg.)	59.30	55.10	50.18	48.48
E_{rm} (GPa)	33.80	33.80	33.80	33.80

This problem is aggravated when a large number of openings are present, and when depth varies strongly from the top to bottom of the model, as is the case with Zawarmala mine. In this case, the intervening pillars show large displacements. This has detrimental effect on the stability of adjacent openings, thereby imparting general instability to the model.

The probable reason for the modelling difficulties experienced with the Roclab™ approach to Hoek–Brown formulations is that, remarkably, increase in the modulus of elasticity with increased confinement with depth is not considered. This aspect is illustrated in Table 8. Under the given stress regimes, σ_3 is calculated for 100, 200, 400, and 500 m of depths below the surface. The other inputs are: $\sigma_{ci}=120$ MPa, $GSI=71$, $m_i=20$, and $E_i=45$ GPa,

From Fig. 1, which was developed over a period of several years of trial-and-error fitting to data on rock quality, deformation modulus, and seismic velocity (including deep cross-hole seismic velocity, where core logging was performed by colleagues at NGI), it can be seen that deformation modulus increases with depth, just as seismic velocity tends to also (Fig. 24). Using a wider range of depths from 25 to 500 m, and $GSI=71$, or $RMR=66$, or $Q\approx 10$ (from the approximation $RMR=50+15\log Q_c$), we see that the following approximate deformation moduli can be expected (Table 9) when using the alternative Q-based model of Ref. [1], rather than the Hoek–Diederich formulation seen at the top of Table 1.

9. Discussion

GSI-based Hoek–Brown formulations of geotechnical input data for rock masses, shown in Table 1, appear to have reached 'black-box' levels of complexity. Furthermore, the very nature of a 'c plus tan φ' formulation, whether as a linear Mohr–Coulomb, or non-linear Hoek–Brown formulation, has been shown by others [7] to be inappropriate for the modelling of the shear strength of *even* rather massive almost un-jointed rock masses, as dramatically demonstrated for the URL mine-by tunnel in Fig. 2. The successful and highly logical 'c *then* tan φ' approach of Ref. [7], demonstrated in Fig. 3, has therefore been followed in principal in this paper.

However, c and φ inevitably have very uncertain magnitudes, certainly unworthy of *any* decimal places. This is because both the intact rock 'bridges' (failing at small strain, with strong dilation), and the shear mobilization along the newly fractured surfaces (at larger strain and with strong dilation at first), plus the contribution of joint sets and discontinuities (with lower degrees of dilation), inevitably make for a complex 'whole-system-behaviour', post-peak, which no one will ever be able to quantify accurately. So do not be misled into assuming any accuracy when seeing endless decimal places.

Please cite this article as: Barton N, Pandey SK. Numerical modelling of two stoping methods in two Indian mines using degradation of c and mobilization of φ based on Q-parameters. Int J Rock Mech Mining Sci (2011), doi:10.1016/j.ijrmms.2011.07.002

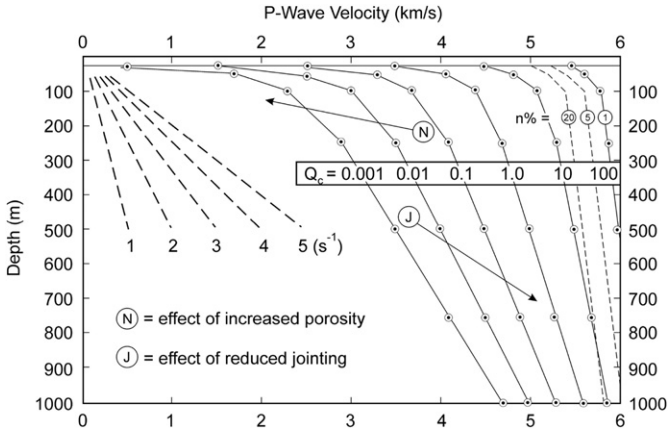

Fig. 24. The above discussion about the need for depth-dependent moduli, which remarkably seem to be absent from 'standard' modelling routines, is emphasised in this conversion of the depth-dependent 'lines' of Q_c and V_P shown in Fig. 1. These 'iso-Q_c' lines show the trends of V_P variation with depth, and they will have inevitable moduli increases with depth [2].

Table 9
Approximate estimates of rock mass deformation modulus increases with depth for $Q=10$, roughly representing RMR=65 and GSI=70.

Depth (m)	25	50	100	250	500
E_{rm} estimate (GPa)	22	28	34	39	46

The writer has often used the 'Chinese method' of rapidly left-thumbing from the back of a consultant's report to the front, whereby the coloured and endless stress distributions and deformation patterns in the appendices can be read almost as in a film. Does this 'colour' represent anything real? Would the numerical modellers know how to input a neglected clay seam—without 'smoothing-it-out' in a continuum approximation? Would the equations for φ' and c' in Table 1 change very much? For these reasons, a much simpler and much more transparent approach is considered acceptable, and thus the simple *CC* and *FC* formulations, already contained in the Q_c formulation, can make an attractive starting point, for *very roughly* estimating the peak values of c and φ.

It has been found from the modelling performed, that certain aspects of observed mine behaviour are more realistically captured in the 'c *then* tan φ' approach, including the modelling result that immediate stope periphery rocks experience tensile stresses in all the stopes (Fig. 9), and that concentration of shear stresses above the stopes causes development of an 'internal' rather than superficial shear band (Fig. 11).

Uneven stress distributions in mines are generally caused by major geological structures such as faults, folds, etc. In their absence, strata are more likely to experience uniform stress distribution, if rock moduli are of similar magnitude. For the Zawar group of mines, the stress magnification due to mining is of the order of 1.8 to 2.2 times the in situ stresses. At a depth of 260 m from the surface, the value of σ_H is approximately 17 MPa. Therefore, the maximum stress concentration due to mining of stope CW-0 (E) would be in range of 30–37 MPa in the horizontal pillar above it. However, in the case of the '$c+\tan\varphi$' approach, the maximum stress at the pillar periphery above stope CW-0 (E) is 55 MPa and the core experiences around 40–45 MPa. On the other hand, the 'c *then* tan φ' approach exhibits a uniform stress distribution of about 40 MPa which is more reasonable in relation to limited observations of stress-induced failure (Figs. 6 and 7).

Similarly, the immediate peripheries of a large (and non-circular) opening must experience tensile stresses. In Fig. 8, not all the openings modelled with the '$c+\tan\varphi$' approach experience tensile stresses. In the mine, a few fallen blocks were observed in all the three stopes, apparently originating from the crown, approximating the maximum block size of $1.8\times1.5\times2.0\,m^3$ ($L\times B\times H$) of the rock mass.

As is known, the stability of a rock mass at shallow depths is governed by its shear strength. Hence the location, magnitude and the direction of an eventual shear band is very important in ascertaining the stability of the opening, whether it is a small tunnel or a large stope. In the case of an opening between two adjacent stopes, thereby experiencing high compressive stresses, failure is observed along a plane dipping approximately 30° to the maximum stress direction.

Similarly, for the rock mass prone to rock burst, the sound is always deep seated indicating shearing along joints or intact rock failure away from the immediate periphery. This is better modelled by the 'c *then* tan φ' approach, where a shear band has developed away from the immediate periphery (Fig. 11). The '$c+\tan\varphi$' approach indicates shear stress concentration in the immediate periphery, contrary to the field observations (Fig. 10).

10. Conclusion and recommendations

1. The failure mode involving rock breakage is highly unlikely to be governed by the Mohr–Coulomb or Hoek–Brown style of strength criterion '$c+\tan\varphi$', because intact rock clearly fails at small strain, breaking 'the cohesion', followed by mobilization of friction along fracture surfaces, joints and discontinuities, at increasingly larger strain. The 'c *then* tan φ' approach is preferred.
2. The various simple equations and correlations proposed, including depth-dependent moduli, can be used with minimum effort to calculate the various input parameters for numerical modelling, with no limit to the problem size and number of excavations.
3. The best feature of using the proposed equations is that one can easily back-calculate the Q value knowing the displacement recorded at a particular location, when the stress regime is roughly known, and the compressive strength also roughly known. This not only diminishes the uncertainties in the parameters but also helps in general understanding of the rock mass behaviour.
4. In transverse stoping, rib pillars experience tensile stresses post stoping. This tensile zone increases with depth and with increase in the in-situ stresses and increase in the rock mass properties. The proposed modelling method seems to mirror this observation.

Acknowledgement

The authors are thankful to the management of HZL, for granting permission to publish this article.

References

[1] Barton N. Some new Q-value correlations to assist in site characterization and tunnel design. Int J Rock Mech Min Sci 2002;39:185–216.
[2] Barton N. Rock quality, seismic velocity, attenuation and anisotropy. London: Taylor & Francis; 2006.
[3] Barton N, Lien R, Lunde J. Engineering classification of rock masses for the design of tunnel support. Rock Mech 1974;6:189–236.
[4] Potvin Y, Milne D. Empirical cable bolt support design. In: Kaiser PK, McCreath DR, editors. Rock Support. Rotterdam: Balkema; 1992. p. 269–75.
[5] Hutchinson DJ, Diederichs MS. Cablebolting in underground mines. Vancouver: Bitech Pub; 1996 416 pp.
[6] ITASCA. Flac 3d manual. Minneapolis: Itasca Consulting; 2006.

Please cite this article as: Barton N, Pandey SK. Numerical modelling of two stoping methods in two Indian mines using degradation of c and mobilization of φ based on Q-parameters. Int J Rock Mech Mining Sci (2011), doi:10.1016/j.ijrmms.2011.07.002

ARTICLE IN PRESS

[7] Hajiabdolmajid V, Martin CD, Kaiser PK. Modelling brittle failure. In: Girard J, Liebman M, Breeds C, Doe T, editors. Proc. 4th North Amer Rock Mech Symp, Seattle. Rotterdam: Balkema; 2000. p. 991–8.
[8] Martin DC, Christiansson R, Soderhall J. Rock stability considerations for siting and constructing a KBS-3 repository, based on experience from Äspö HRL, AECL's HRL, tunnelling and mining. Stockhom: SKB (Swedish Nuclear Fuel Co); 2001, Rep TR-01-38.
[9] Grimstad E, Barton N. Updating of the Q-System for NMT. In: Proceedings of the International Symposium on Sprayed Concrete, Fagernes, Norway. Oslo: Norweg Concr Assoc; 1993.
[10] Barton N, Grimstad E. The Q-system following twenty years of application in NMT support selection. Felsbau 1994;6:428–36.
[11] Hoek E, Brown ET. Practical estimates of rock mass strength. Int J Rock Mech Min Sci 1997;34(8):1165–86.
[12] Edelbro C. Numerical modelling of observed fallouts in hard rock masses using an instantaneous cohesion-softening friction-hardening model. Tunnell Undergr Space Tech 2009;24(4):398–409.
[13] Zhao XG, Cai M. A mobilized dilation angle model for rocks. Int J Rock Mech Min Sci 2010;47:368–84.
[14] Barton N, Choubey V. The shear strength of rock joints in theory and practice. Rock Mech 1977;1/2:1–54.
[15] Barton N, Bandis, S. Effects of block size on the shear behaviour of jointed rock. In: Proceedings of the 23rd US Rock Mechanics Symposium, Berkeley, Calif; 1982. p. 739–60.

Please cite this article as: Barton N, Pandey SK. Numerical modelling of two stoping methods in two Indian mines using degradation of c and mobilization of φ based on Q-parameters. Int J Rock Mech Mining Sci (2011), doi:10.1016/j.ijrmms.2011.07.002